Modelling and Bifurcation Analysis of Germinal Center Dynamical System

Jared Frazier
Course: University of Amsterdam, Bioinformatics I
Program: MSc. Computational Science
Email: jared.frazier@student.uva.nl
Student ID: 14322234
Date: 2023-10-29

Abstract: In this report, the germinal center (GC) exit pathway, whose mechanisms are critical for understanding the immune response, was modeled as a system of ordinary differential equations [1]. The system was first decomposed into two relevant subnetworks, and steady state analysis of key transcription factors relevant for the terminal differentiation of naive GC B cells to short term immune response plasma cells (PCs) or long term immune response memory B cells (MBCs) was performed. Associated bifurcation analyses and system phase spaces were used to elucidate the conditions under which the differentiation of naive GC B cells (aka centroblasts) to MBCs or PCs occurred.

1. Introduction

1.1. Overview

Germinal centers (GCs) are distinct regions in secondary lymphoid tissues (lymph nodes, spleen, etc.) where affinity maturation, the process whereby antibodies are produced with strong binding properties to antigens, of B cell clones (copies of B lymphocytes–aka B cells–that mature in bone marrow and express antigen-binding receptors on their membranes) occurs [2–4]. GCs form approximately one week after exposure to antigen, and they are composed of two spatially segregated compartments: the light zone (LZ) and the dark zone (DZ) [2, 5]. The DZ is the primary site of somatic hypermutation (SHM) in which largely random mutations of gene segments of B cells occurs [3]. The LZ is where B cells test their antigen receptors against antigens retrieved on follicular dendritic cells (FDCs) [6]. The subsequent B cell receptor (BCR) binding to antigens facilitates the formation of structures that allow the B cell to receive help from T follicular helper cells (TFHs) [6]. This is known as postive selection, and the iterative rounds of mutation and selection of B cells in the LZ and DZ produce high-affinity antibody secreting plasma cells (PCs) and memory B cells (MBCs) [5, 6]. Ultimately, an understanding of the mechanisms of GC responses to pathogens forms a critical framework for vaccination in which the magnitude and quality of GC response influence long-term humoral immunity [5–7].

1.2. Plasma Cell Differentiation

1.2.1. TFH Cells

In this section, the role of TFH cell in selection and generation of PCs is summarized. The key question that [5] proposes here is what are the mechanisms that signal the initiation of PC differentiation. The studies proposed by [5] suggest that the positive selection and generation of PCs occur such that BCR stimulation and TFH cell signaling are independent of one another. TFH-cells facilitate PC production and this was suggested by experiments in which antigen was delivered to GC B cell via the surface receptor DEC-205 [5]. It is, moreover, known that a number of signaling lymphocyte activation molecules (SLAM) are expressed on TFH cells, and that SLAM-associated protein (SAP) is essential for the generation of both MBCs and PCs [8]. It is, therefore, clear that TFH cells play a critical role in PC differentiation (PCs themselves playing a significant role in adaptive immune response) [9]. However, what is important to note about what is claimed to be known is that these claims are based upon data that may also indicate other signaling molecules involvement in PC differentiation [5].

1.2.2. BCR Signaling

While several studies suggest that BCR signaling may be important in driving PC differentiation, experiments conducted by [5] yielded contradictory results. Despite these contradictory results, *ex vivo* analysis of GC B cells indicated that GC B cells undergo BCR signaling; however, *in vivo* results show that highly proliferative GC B cells–those that are rapidly dividing and differentiate into PCs and MBCs–do not undergo BCR signaling except during a particular cell phase [5, 10]. The model that follows from these data integrates both BCR and TFH cell

signaling to achieve activation and selection of GC B cells, and their subsequent differentiation to PCs. It is important to note that it is unclear whether antigen engagement, which promotes PC differentiation, is the result of BCR signaling [5]. Lastly, the transcriptional regulator B-lymphocyte-induced maturation protein-1 (Blimp1) induces the expression of X-box binding protein (XBP-1), which is required for PC differentiation [5, 11]. The CXRC4 and IRF4 transcription factors also facilitate migration of GC B cells through the DZ and expression/repression of GC B cells, respectively.

1.3. Memory B Cell Differentiation.

As in the previous section wherein confounding variables obfuscate the roles of TFH cells and BCR signaling in PC differentiation, MBCs could be GC-derived or GC-independent (Bcl6 deficient MBCs that did not undergo somatic mutations and thus affinity maturation, which is what occurs for GC-derived MBCs) [5, 12]. A consistent characteristic of MBCs is that they have low antigen affinity compared to PCs [5]. In particular, a recent study suggests that BACH2 expression is a "fate-determining" transcription factor for the differentiation of GC B cells to MBCs; however, it is worth noting that GC B cells that lacked CXCR4, and could not access the DZ, were also more likely to enter the MBC compartment [5, 13]. Notably, MBCs express similar chemokine (proteins that are known to promote the migration of cells) profile to naive B cells, which coincides with the role of MBCs in residing in tissues and protecting against antigens in the long term [5, 14].

1.4. Summary

Following an immune response, two types of differentiated B cells form: PCs, which confer immediate protection from antibodies, and MBCs, which confer long term protection against antibodies [15]. Understanding the mechanisms by which differentiation of B cells into PCs and MBCs occurs is crucial, and the model proposed in [5] suggests that within the GC, there are distinct roles performed by certain transcription factors, signaling mechanisms, and cell (e.g., TFH) help in the selection and differentiation of variable antigen affinity cells from GC B cells [16]. Thus, the mechanisms in the GC that correspond with the GC B cell differentiation to MBCs and PCs, each with different antigen specificity, in the immune response yield an elegant model mediated by reasonably well-defined processes [5].

In the current report, the differentiation of GC B cells to PCs is modelled using a dynamical system model proposed in previous work [1]. Particular emphasis is made on reproducing key figures regarding the stability of terminal states of the dynamical system, that is under what conditions the GC B cells differentiate to MBCs or PCs [1].

2. Methods

Equations (1) - (7) describe the GC exit pathway using ordinary differential equations (ODEs). Equations (1) - (3) describe the protein levels for BLIMP1 (p), BCL6 (b), and IRF4 (r), respectively, and they assume that the protein level for each transcription factor is proportional to the mRNA levels. Equations (4) and (5) denote regulatory signals coming from surface receptors of GC B cells. Note that equations (6) and (7) are time t forced Gaussian probability density functions (PDFs) with several parameters denoting the signaling strength of BCR_{max} and $CD40_{max}$, the spread of the time period σ_{BCR} and σ_{CD40} over which signaling occurs, as well as the center of the PDFs at μ_{BCR} and μ_{CD40}. While equations (6) and (7) define parameterized functions for surface signaling, bcr_0 and cd_0 may also be treated as constant parameters of the model. Due to this potential confusion, it is explicitly stated throughout the report whether findings/figures were generated using the Gaussian bcr_0 and cd_0 signaling or not. The remaining parameters in equations (1) - (3) are μ_f, σ_f, k_f, and λ_f that represent basal transcription rate, maximum induced transcription rate, dissociation constants, and degradation rates, respectively, for transcription factors $f \in \{p, b, r\}$. The model is described in greater detail in previous work and the default parameters from the same work were used in the current report unless otherwise specified [1].

$$\frac{dp}{dt} = \mu_p + \sigma_p \frac{k_b^2}{k_b^2 + b^2} + \sigma_p \frac{r^2}{k_r^2 + r^2} - \lambda_p p \tag{1}$$

$$\frac{db}{dt} = \mu_b + \sigma_b \frac{k_p^2}{k_p^2 + p^2} \frac{k_b^2}{k_b^2 + b^2} \frac{k_r^2}{k_r^2 + r^2} - (\lambda_b + BCR)b \tag{2}$$

$$\frac{dr}{dt} = \mu_r + \sigma_r \frac{r^2}{k_r^2 + r^2} + CD40 - \lambda_r r \tag{3}$$

$$BCR = bcr_0 \frac{k_b^2}{k_b^2 + b^2} \tag{4}$$

$$CD40 = cd_0 \frac{k_b^2}{k_b^2 + b^2} \tag{5}$$

$$bcr_0 = BCR_{max} \frac{1}{\sigma_{BCR}\sqrt{2\pi}} \exp[-\frac{1}{2}(\frac{t - \mu_{BCR}}{\sigma_{BCR}})^2] \tag{6}$$

$$cd_0 = CD40_{max} \frac{1}{\sigma_{CD40}\sqrt{2\pi}} \exp[-\frac{1}{2}(\frac{t - \mu_{CD40}}{\sigma_{CD40}})^2] \tag{7}$$

Before modelling the entire system, a submodule of the GC exit pathway called the BCR subnetwork was investigated in order to quantify the early dynamics of GC B cells. Equations (8) and (9) define this BCR subnetwork, and are similar to equations (1) and (2), however, to interrogate the early system dynamics, terms involving IRF4, which is expressed at a later stage, were removed.

$$\frac{dp}{dt} = \mu_p + \sigma_p \frac{k_b^2}{k_b^2 + b^2} - \lambda_p p \tag{8}$$

$$\frac{db}{dt} = \mu_b + \sigma_b \frac{k_p^2}{k_p^2 + p^2} \frac{k_b^2}{k_b^2 + b^2} - (\lambda_b + bcr_0 \frac{k_b^2}{k_b^2 + b^2})b \tag{9}$$

To interrogate these early system dynamics, steady-state (nullcline analysis) exploration of the BCL6 and BLIMP1 expression levels as well as bifurcation analysis of bcr_0 with varied transcription and degradation rates of BCL6 were performed. Equations (10) and (11) are functions that arise from setting the BLIMP1 and BCL6 time differentiated state variables to zero and subsequently solving for BLIMP1 (p) in both cases. Thus, the nullclines $n_p(b)$ and $n_b(b)$ for BLIMP1 and BCL6, respectively, are both functions of BCL6. The derivation for equation (11) is provided in the supplementary material by equations (S1) - (S8). For these simulations, bcr_0 and cd_0 were not modelled as Gaussian PDFs. Instead, bcr_0 was used as a smoothly changing bifurcation parameter on the interval $[0, 30]$.

$$\frac{dp}{dt} = 0 \Leftrightarrow n_p(b) = p = \frac{\mu_p + \sigma_p \frac{k_b^2}{k_b^2 + b^2}}{\lambda_p} \tag{10}$$

$$\frac{db}{dt} = 0 \Leftrightarrow n_b(b) = \sqrt{\frac{k_p^2}{[(\lambda_b + bcr_0 \frac{k_b^2}{k_b^2 + b^2})b - \mu_b]\frac{k_b^2 + b^2}{\sigma_b k_b^2}} - k_p^2} \tag{11}$$

In the same vein, bifurcation analysis of the CD40 subnetwork, which is modelled by equation (3) was performed. Because CD40 is dependent on the protein level of BCL6 in equation (5), it was assumed that $CD40 = cd_0$ for the purpose of the bifurcation analysis. The CD40 subnetwork is defined in equation (12).

$$\frac{dr}{dt} = \mu_r \sigma_r * \frac{r^2}{k_r^2 + r^2} + cd_0 - \lambda_r r \tag{12}$$

With submodules of the GC dynamical system investigated, a bifurcation study of BCL6 for each of the system parameters μ_f, σ_f, k_f, and λ_f was performed in order to qualitatively evaluate which parameters resulted in significant changes in system steady state and the stability of those steady states. For these simulations, bcr_0 and cd_0 were not modelled as Gaussian PDFs, but rather were parameters of the model.

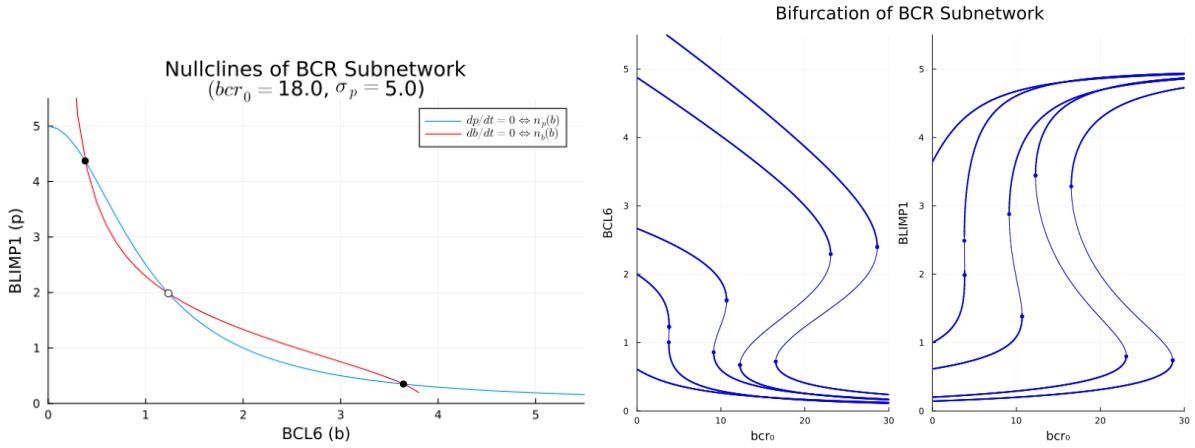

(a) (b)

Fig. 1: Nullclines (a) and bifurcations about the parameter bcr_0 (which is not Gaussian) (b) of the BCR subnetwork. The five curves for each subplot in (b) are bifurcation curves for $(\mu_b, \lambda_b) \in \{(1,10),\ (0,5),\ (1.75,4),\ (1,1),\ (3,1)\}$. The thinner blue line between the two points are unsteady fixed points. Note that cd_0 is also not Gaussian for these simulations.

With constant bcr_0 and cd_0 simulation conducted, the dynamics of the system using the more realistic Gaussian PDF formulation was lastly investigated. Since GC B cells can differentiate to MBCs or PCs, IRF4-mediated activation of BLIMP1 in equation (1) was abrogated and the dynamical system was evolved accordingly to quantify the steady state of the system under these conditions which have been hypothesized by previous work to facilitate MBC differentiation [1]. Moreover, to quantify the steady state of BCL6 under the more realistic Gaussian formulation of *BCR* and *CD*40 signaling, a bifurcation study of BCL6 for bcr_0 and cd_0 as the *implicit* bifurcation parameters was performed. The *explicit* bifurcation parameter, that is the parameter that smoothly changes on a designated interval, was actually the timestep t that is used as an argument to the forced signaling functions described by equations (6) and (7). These fixed points were thus computed using root finding methods for which the parameter values of bcr_0 and cd_0 were determined by the timestep t and the corresponding equations.

Lastly, the Julia programming language was used to implement all numerical simulations. The `DynamicalSystems.jl`, `ChaosTools.jl`, and `BifurcationKit.jl` libraries formed the basis for trajectory computation of the system, fixed point analysis, and bifurcation analysis, respectively.

3. Results

The steady state analysis of the BCR subnetwork and associated bifurcation analysis is shown in figure 1. Figure 1a shows the nullclines, that is the steady state of the system converted to function form, for a range of BCL6 protein levels. The intersections of the nullclines, by definition, represent fixed points of the system. The two black dots represent a stable fixed point and the white dot represents an unstable fixed point. To complement the nullcline analysis, figure 1b shows the qualitative changes in the fixed points of both state variables in the BCR subnetwork. The BCL6 bifurcation curve that intersects with the y-axis at c.a. 0.6 and the BLIMP1 bifurcation curve intersecting with the y-axis at c.a. 3.8 corresponds to the parameter set $(\mu_b, \lambda_b) = (1,10)$. Reading from left to right in the parameter set $(\mu_b, \lambda_b) \in \{(1,10),\ (0,5),\ (1.75,4),\ (1,1),\ (3,1)\}$ corresponds to an increase in the value of the y-axis intersection for the BCL6 bifurcation curves and a decrease in the value of the y-axis intersection for the BLIMP1 bifurcation curves. Unstable fixed points for these bifurcation curves in figure 1b correspond to only $(\mu_b, \lambda_b) \in \{(0,5),\ (1.75,4),\ (1,1),\ (3,1)\}$.

With the BCR subnetwork analyzed, the full model has been also decomposed into a CD40 subnetwork and bifurcation analysis of this ODE was performed. Figure 2 shows the results of this bifurcation analysis for two sets of parameter regimes. Figure 2a shows two saddle-node bifurcations in between which there are only unstable fixed points. Figure 2b shows only a single saddle-node bifurcation. The parameters listed above each subplot in figure 2 correspond to the IRF4 parameters as well as the initial cd_0 that was used for the numerical continuation algorithm initial guess—numerical continuation algorithms incorporate root finding algorithms that require such an initial guess when computing the depicted fixed point curves. The parameter β is a bistability related parameter and theoretically corresponds to certain regimes in the fixed point space [1].

Having analyzed the subnetworks composing the GC exit pathway model defined by equations (1) - (3), to

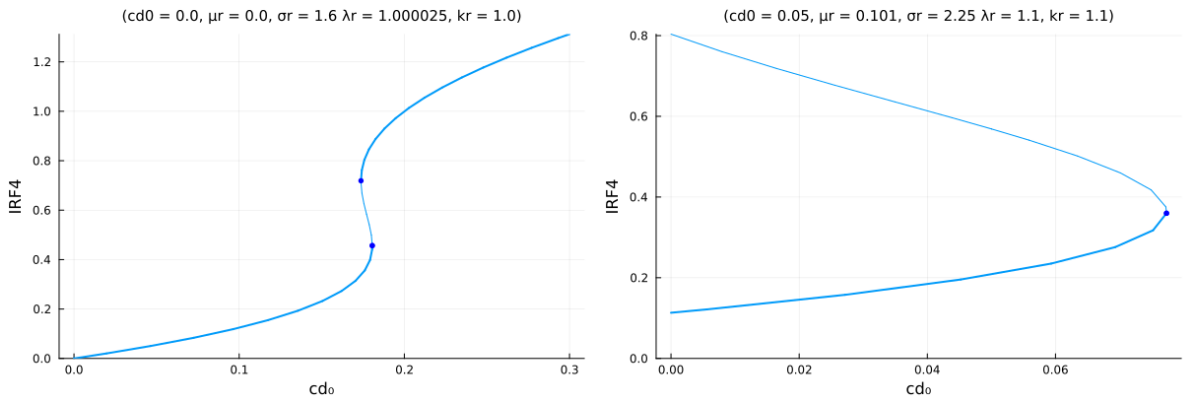

(a) (b)

Fig. 2: Bifurcation of IRF4 subnetwork about cd_0 for two different parameter regimes. (a) Bifurcation of cd_0 for a set of IRF4 parameters that theoretically lay outside of the bistable switch regime ($\beta = 1.6$). The thinner blue line between the two points are unsteady fixed points. (b) Bifurcation of cd_0 for a set of parameters that theoretically produce terminal PC or GC B cell steady states ($\beta = 1.98$). The thinner blue line above the point are unsteady fixed points.

interrogate the sensitivity of BCL6 to all system parameters, a bifurcation analysis of system parameters was performed and is shown in figure 3. The points in each diagram are fixed points of the system evolving for the smooth change of each parameter. Parameters for IRF4, that is μ_r, σ_r, λ_r, and k_r, show saddle-node bifurcations and corresponding unstable fixed points. The remaining parameters do not have any such branching points, and thus contribute to only stable fixed points (a so-called monostable regime).

Previous results only account for bcr_0 and cd_0 that are considered constant parameters of the model. This is not a realistic representation of the actual surface signaling dynamics, so in figure 4 the trajectories of the transcription factors subject to Gaussian forced bcr_0 and cd_0 are shown. The decrease in BCL6 due to the peaking of BCR (the signaling for which is shown in the inset of fiure 4) also corresponds with the small increase in the BLIMP1 protein level. This is straightforward to see from a mathematical perspective since BCR suppresses BCL6 expression in equation (2) and as BCL6 decreases the hill function $\frac{k_b^2}{k_b^2+b^2}$ in equation (1) increases, thus BLIMP1 expression also increases. Moreover, the thick lines correspond to a hypothetical system for which MBC differentiation is expected, and it is claer that the steady state of such a system has far lower BLIMP1 (blue line) protein levels when compared with the system for which PC differentiation is expected.

Having shown a phase space in which MBC and PC differentiation occurs, the sensitivity of the GC exit pathway, specifically BCL6, to two bifurcation parameters bcr_0 and cd_0 modelled by Gaussian PDFs was explored. Figure 5 shows four different bifurcation diagrams where the fixed points correspond to BCL6 levels at different levels of bcr_0 and/or cd_0 signalling. Since bcr_0 and cd_0 were modelled using Gaussian PDF, the values of bcr_0 and/or cd_0 are shown as a function of time. The bifurcation diagrams, therefore, correspond to a "snap-shot" in time at a particular level of BCR and CD40 signaling and the associated BCL6 fixed point at that time. As with previous plots, an unstable fixed point regime is shown in figures 5a and 5b.

The fixed points in figure 5 can be more easily understood in the context of an example trajectory with and without CD40 signaling. Figure 6 shows such example trajectories and is meant to clarify the annihilation of fixed points that occurs in figure 5 as CD40 signaling begins to overlap with BCR signaling. Essentially, two example steady states are shown for BCL6 where BCL6 levels without CD40 returns to levels prior to stimulation while BCL6 with CD40 signaling reaches a steady state with significantly lower levels. The insets in figure 6 correspond to the Gaussian PDFs associated with bcr_0 and cd_0 as well as the actual BCR and CD40 levels corresponding to equations (4) and (5), respectively.

4. Discussion

By separating the GC model into a BCR subnetwork and an IRF4 subnetwork, insights regarding the steady states of these two submodules indicate the separate importance of BLIMP1, BCL6, and IRF4 in differentiation of GC B cells. In figure 1a, a bistable regime characterized by low BCL6 and high BLIMP1 as well as high BCL6 and low BLIMP1 was demonstrated. The unstable fixed point is not biologically observable; however, the two stable fixed points appear to be reachable from increasing or decreasing levels of BCR stimulation, which is depicted

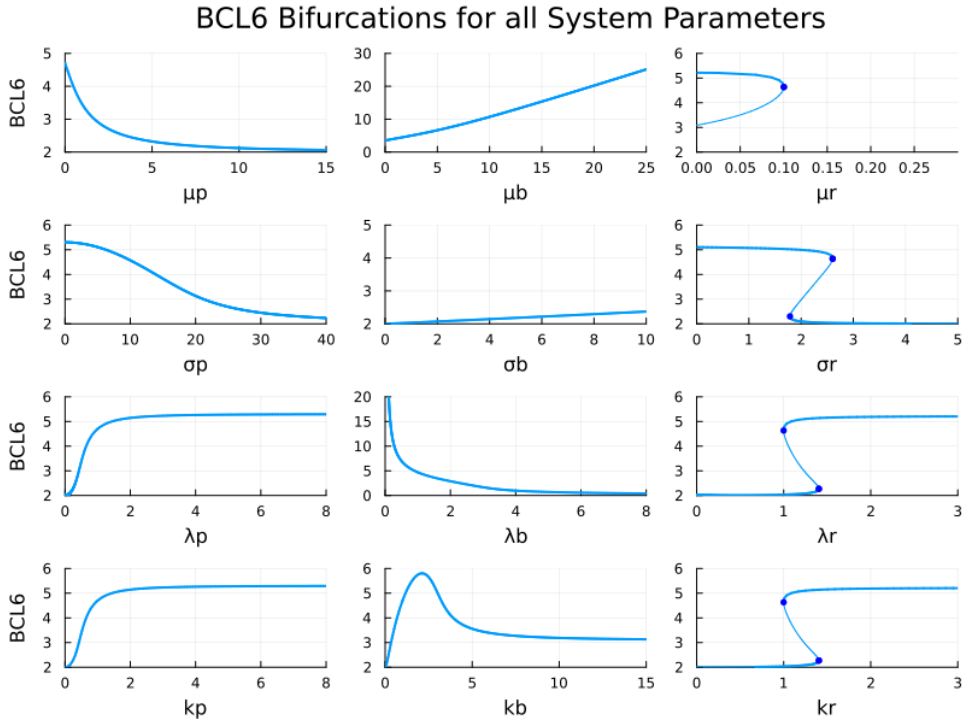

Fig. 3: BCL6 bifurcation study of equations (1) - (3) for all parameters and with constant $bcr_0 = 0$ and $cd_0 = 0$. The thinner line between or below the points in the 3^{rd} column of the figure are unstable fixed points.

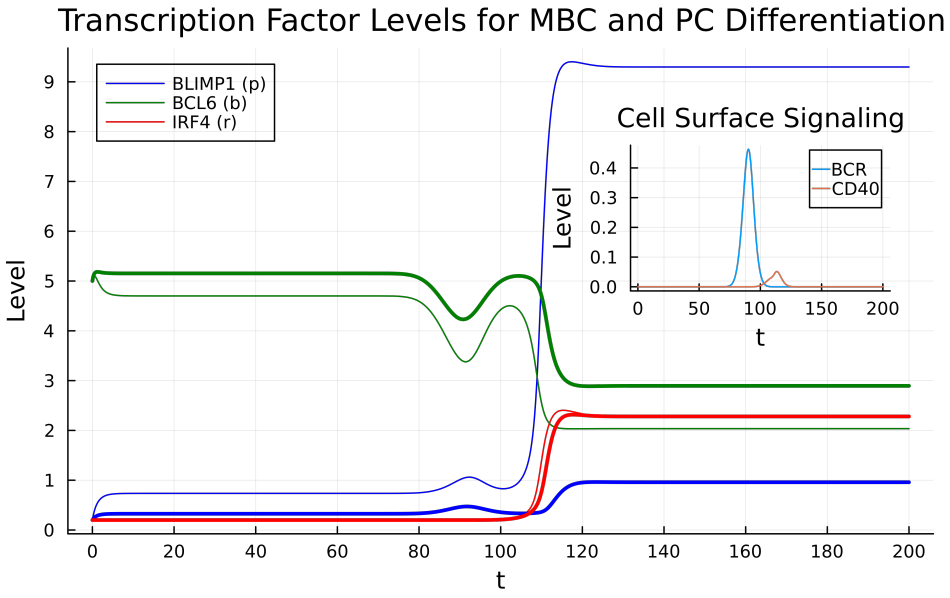

Fig. 4: Memory B Cell (MBC) differentiation compared to plasma cell (PC) differentiation with Gaussian bcr_0 and cd_0 signaling. The thick lines represent the evolution of the protein levels in a GC system for which IRF4-mediated activation of BLIMP1 has been abrogated.

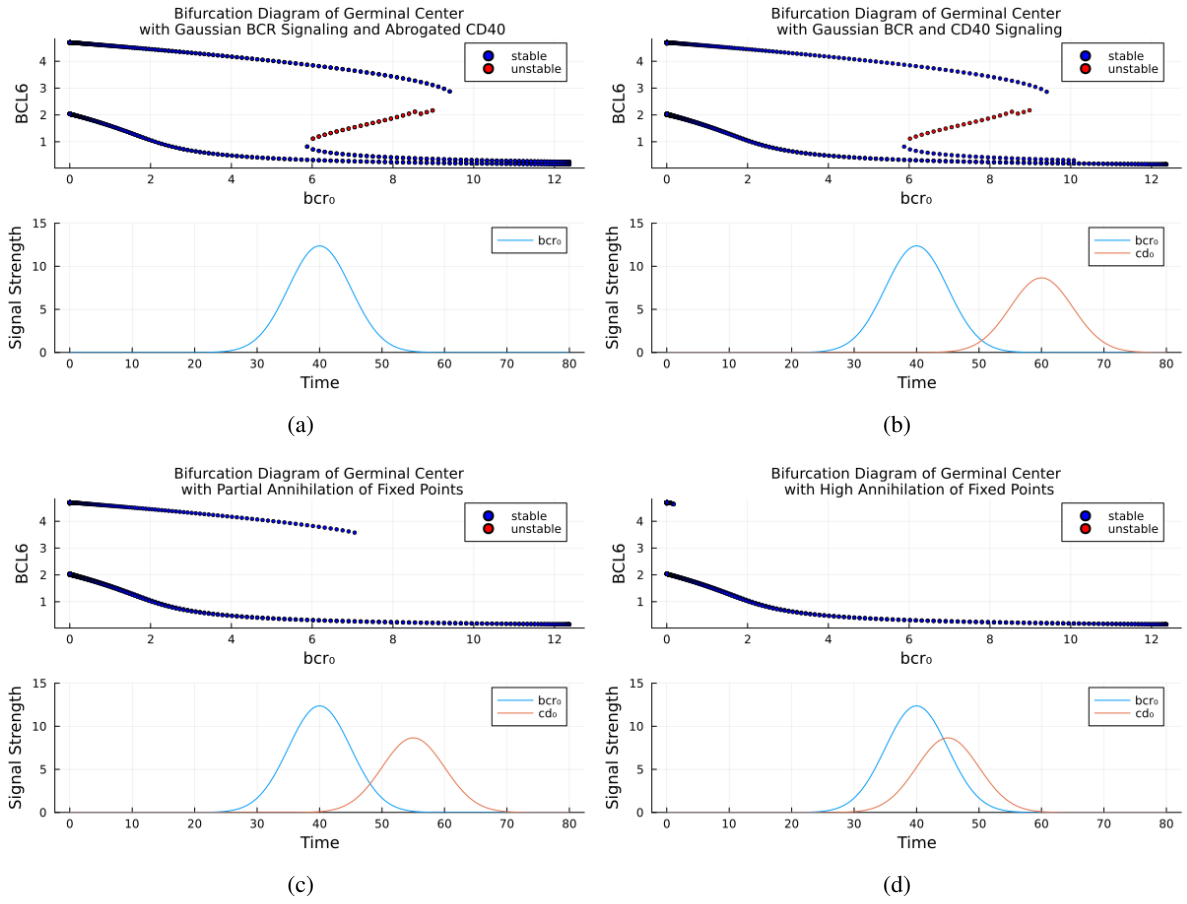

Fig. 5: Bifurcation study of BCL6 subject to forced Gaussian PDFs for bcr_0 and cd_0 described by equations (6) and (7), respectively. (a) BCL6 steady states with abrogated CD40 signaling. (b) BCL6 steady states with minimally overlapping BCR and CD40 signaling. (c) BCL6 steady states with partially overlapping BCR and CD40 signaling. (d) BCL6 steady states with high overlapping BCR and CD40 signaling.

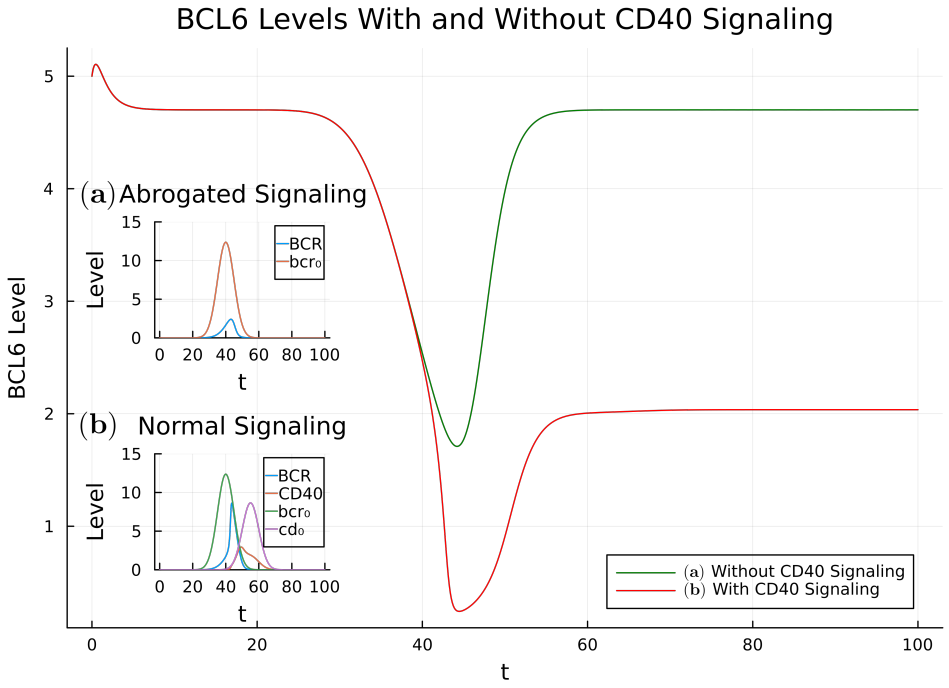

Fig. 6: Two example trajectories for BCL6 in a GC model with BCR signaling and abrogated CD40 signaling in inset (**a**) as well as in a GC model with BCR signaling with CD40 signaling (normal signaling) in inset **(b)**. Inset **(a)** corresponds to the same signaling distribution as figure 5a while inset **(b)** corresponds to the same signaling distributions as figure 5c.

by the bifurcation curves in figure 1b. Thus, the BCR subnetwork alone does not demonstrate the irreversibility that is associated with naive B cell differentiation to plasma cells or memory B cells. It is worth noting that the nullclines were computed analytically, the derivation for this is shown in equations S1 - (S8). The resulting nullclines are not in agreement with a previous report; however, upon computing nullclines numerically using the R package `phaseR` as shown in figure S1, the behavior in a previous report is more closely replicated [1]. While not necessarily of biological significance, this provides some insight regarding the potential importance methodological differences with respect to phase space analysis in general.

Similarly, figure 2a shows another reversible bistable regime related to the simulation of CD40, and under a different parameter regime in figure 2b it appears that only low levels of IRF4 are attainable as steady states. This disagrees with bifurcations of IRF4 with respect to varied CD40 levels shown in previous work, and also disagrees with theoretical findings in the same report; however, since not all parameters are provided in the previous work, it is difficult to exactly replicate the intended behavior [1].

While the submodules provide some insights regarding steady states, the importance of the two submodules relative to the entire GC kinetic model is demonstrated in figure 3. In figure 3, only the parameters associated with IRF4 lead to qualitative changes in the dynamics of BCL6 that support bistable switching. This is primarily because the alteration of other parameters results in only stable fixed point regimes for BCL6; however, it is claimed that BCL6 plays an important role in the terminal differentiation of naive B cells, and given that bistability is shown in column three of figure 3, this indicates also the joint importance of IRF4 on terminal differentiation of these B cells [1].

In the context of constant bcr_0 and cd_0, the realistic dynamics of the GC model are ignored. To investigate more realistic dynamics, figure 4 shows two different differentiation outcomes for a naive GC B cell resulting from Gaussian regulated BCR and CD40 signaling mechanisms. Previous work posits that high BLIMP1 levels are associated with plasma cell differentiation, and this can also be justified from a qualitative perspective based on positive feedback mechanisms associated with BLIMP1 expression, [1]. On the contrary, low BLIMP1 levels are associated with MBC differentiation. These two differentiation states are shown in figure 4 since the abrogation of IRF4 contribution to BLIMP1 expression, that is the limiting of this positive feedback mechanism, leads to a BLIMP1 steady state that is far below that of the IRF4 mediated BLIMP1 levels.

Lastly, the fate of GC B cells is shown as a bifurcation of BCL6 about different BCR and CD40 signaling regimes in figure 5 and figure 6. Figure 5b would suggest that even with CD40 signaling, there is still reversibility

between the GC B cell and its differentiation to a plasma cell. This is because if one follows the fixed point curve in figure 5b, it would be expected that as BCR levels decrease from 10 to 0, hysteresis would allow BCL6 levels to jump from 1 back to 3.5 and subsequently allow BCL6 levels to return to their state prior to stimulation. This would disagree with experimental and modelled findings in previous work, so in order to investigate the BCL6 dynamics with a more concrete example, a phase space is shown in figure 6 for abrogated and included CD40 signaling corresponding to figure 5a and 5c, respectively. What figure 6 shows actually does agree with the expected results for BCL6 stimulation. The green curve shows BCL6 levels without CD40 signaling, and it is clear that BCL6 returns to its levels prior to stimualtion of BCR. This maps correctly to the bifurcation curve in figure 5a because that curve suggests that decrease of BCR levels (which is approximated with bcr_0 in the figure) may allow a "jump" between lower BCL6 levels and higher BCL6 levels. Conversely, with CD40 signaling, the plasma cell state associated with low levels of BCL6 resulting from negative feedback mechanisms of IRF4 and BLIMP1 expression is shown as the red line in figure 6. The insets of these figures show that while figure 5 has smooth Gaussians for bcr_0 and cd_0, it is important to note that the actual BCR and CD40 signaling curves will not be exaclty Gaussian as they are scaled by a hill function (see equations (4) and (5)).

The decomposition of the GC model to submodules and subsequent introduction of realistic dynamics in the form of Gaussian bcr_0 and cd_0 signaling provides insights into the terminal differentiation mechanisms of GC B cells to MBCs or PCs. While several challenges were encountered in modelling and simulating the GC, the work presented in this report largely agrees with major findings of previous work [1].

References

1. M. R. Martínez, A. Corradin, U. Klein, M. J. Álvarez, G. M. Toffolo, B. Di Camillo, A. Califano, and G. A. Stolovitzky, "Quantitative modeling of the terminal differentiation of B cells and mechanisms of lymphomagenesis," *Proceedings of the National Academy of Sciences of the United States of America*, vol. 109, no. 7, pp. 2672–2677, Feb. 2012.
2. G. D. Victora and M. C. Nussenzweig, "Germinal centers," *Annual Review of Immunology*, vol. 30, no. 1, pp. 429–457, 2012.
3. J. Punt, J. Owen, S. Stranford, and P. Jones, *Kuby Immunology*. W.H. Freeman/Macmillan Learning, 2018.
4. "Immune system — microbes and the human body — microbiology society." [Online]. Available: https://microbiologysociety.org/why-microbiology-matters/what-is-microbiology/microbes-and-the-human-body/immune-system.html
5. D. Suan, C. Sundling, and R. Brink, "Plasma cell and memory b cell differentiation from the germinal center," *Current Opinion in Immunology*, vol. 45, pp. 97–102, 4 2017.
6. R. Nakagawa and D. P. Calado, "Positive selection in the light zone of germinal centers," *Frontiers in Immunology*, vol. 12, p. 661678, 3 2021.
7. H. H. Tam, M. B. Melo, M. Kang, J. M. Pelet, V. M. Ruda, M. H. Foley, J. K. Hu, S. Kumari, J. Crampton, A. D. Baldeon, R. W. Sanders, J. P. Moore, S. Crotty, R. Langer, D. G. Anderson, A. K. Chakraborty, and D. J. Irvine, "Sustained antigen availability during germinal center initiation enhances antibody responses to vaccination," *Proceedings of the National Academy of Sciences*, vol. 113, pp. E6639–E6648, 10 2016.
8. S. Crotty, "T follicular helper cell differentiation, function, and roles in disease," *Immunity*, vol. 41, p. 529, 10 2014.
9. H. C. Allen and P. Sharma, "Histology, plasma cells," *StatPearls*, 12 2022.
10. C. Young and R. Brink, "The unique biology of germinal center b cells," *Immunity*, vol. 54, no. 8, pp. 1652–1664, 2021.
11. S. Nadeau and G. A. Martins, "Conserved and unique functions of blimp1 in immune cells," *Frontiers in Immunology*, vol. 12, p. 805260, 1 2022.
12. T. Takemori, T. Kaji, Y. Takahashi, M. Shimoda, and K. Rajewsky, "Generation of memory b cells inside and outside germinal centers," *European journal of immunology*, vol. 44, pp. 1258–1264, 2014.
13. Q. Hu, T. Xu, M. Zhang, H. Zhang, Y. Liu, H. bing Li, C. Chen, J. Zheng, Z. Zhang, F. Li, N. Shen, W. Zhang, A. Melnick, and C. Huang, "Diverging regulation of bach2 protein and rna expression determine cell fate in early b-cell response," *Cell reports*, vol. 40, p. 111035, 7 2022.
14. C. E. Hughes and R. J. Nibbs, "A guide to chemokines and their receptors," *The Febs Journal*, vol. 285, p. 2944, 8 2018.
15. "Human b cell memory," *Current Opinion in Immunology*, vol. 21, p. 298, 6 2009.
16. A. K. E. Palm and C. Henry, "Remembrance of things past: Long-term b cell memory after infection and vaccination," *Frontiers in immunology*, vol. 10, p. 1787, 7 2019.

Supplementary Material

The derivation of the nullcline for equation (9) is given below for completeness.

$$\frac{db}{dt} = \mu_b + \sigma_b \frac{k_p^2}{k_p^2+p^2}\frac{k_b^2}{k_b^2+b^2} - (\lambda_b + bcr_0\frac{k_b^2}{k_b^2+b^2})b \tag{S1}$$

$$0 = \frac{db}{dt} \tag{S2}$$

$$0 = \mu_b + \sigma_b \frac{k_p^2}{k_p^2+p^2}\frac{k_b^2}{k_b^2+b^2} - (\lambda_b + bcr_0\frac{k_b^2}{k_b^2+b^2})b \tag{S3}$$

$$(\lambda_b + bcr_0\frac{k_b^2}{k_b^2+b^2})b = \mu_b + \sigma_b \frac{k_p^2}{k_p^2+p^2}\frac{k_b^2}{k_b^2+b^2} \tag{S4}$$

$$(\lambda_b + bcr_0\frac{k_b^2}{k_b^2+b^2})b - \mu_b = \sigma_b \frac{k_p^2}{k_p^2+p^2}\frac{k_b^2}{k_b^2+b^2} \tag{S5}$$

$$[(\lambda_b + bcr_0\frac{k_b^2}{k_b^2+b^2})b - \mu_b]\frac{k_b^2+b^2}{\sigma_b k_b^2} = \frac{k_p^2}{k_p^2+p^2} \tag{S6}$$

$$k_p^2 + p^2 = \frac{k_p^2}{[(\lambda_b + bcr_0\frac{k_b^2}{k_b^2+b^2})b - \mu_b]\frac{k_b^2+b^2}{\sigma_b k_b^2}} \tag{S7}$$

$$\frac{db}{dt} = 0 \Leftrightarrow p = \boxed{n_b(b) = \sqrt{\frac{k_p^2}{[(\lambda_b + bcr_0\frac{k_b^2}{k_b^2+b^2})b - \mu_b]\frac{k_b^2+b^2}{\sigma_b k_b^2}} - k_p^2}} \tag{S8}$$

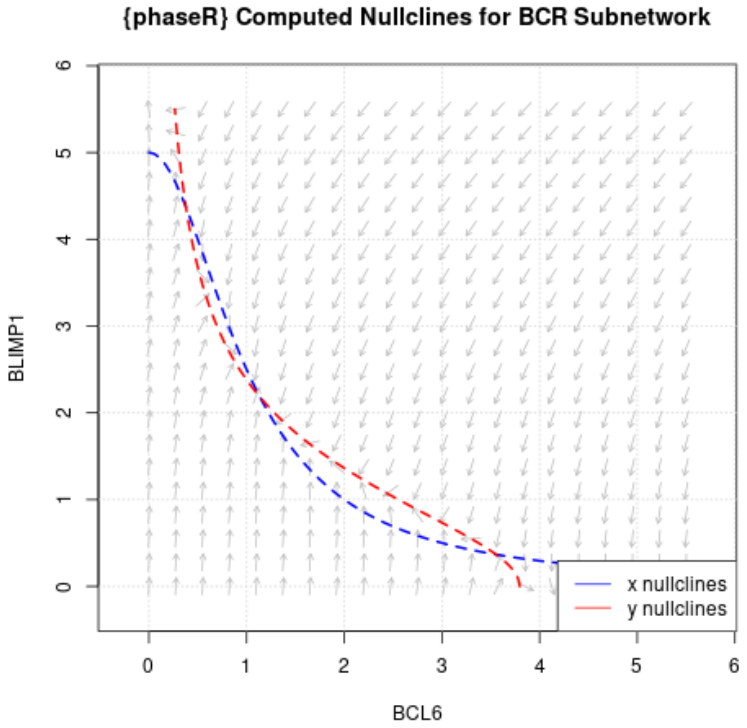

Fig. S1: Numerically computed nullclines using `phaseR` for the BCR subnetwork (equations (8) and (9)).